Chapter

Ultrafast Electron Microscopy with Relativistic Femtosecond Electron Pulses

Jinfeng Yang

Abstract

An ultrafast electron microscope (UEM) with a femtosecond temporal resolution is a "dream machine" desired for studies of ultrafast structural dynamics in materials. In this chapter, we present a brief overview of the historical development of current UEMs with nonrelativistic electron pulses to illustrate the need for relativistic-energy electron pulses. We then describe the concept and development of a UEM with relativistic femtosecond electron pulses generated by a radio frequency (RF) acceleration-based photoemission gun. The technique of RF electron gun and physical characteristics of the relativistic electron pulses are described. Demonstrations of UEM images acquired using approximately 100 fs long electron pulses with energies of 3 MeV are presented. Finally, we report a single-shot diffraction imaging methodology in the UEM with a relativistic femtosecond electron pulse for studies of laser-induced ultrafast phenomena in crystalline materials.

Keywords: ultrafast electron microscopy, ultrafast electron diffraction, femtosecond electron pulse, relativistic electron beam, structural dynamics, radio-frequency electron gun

1. Introduction

It is well-known that transmission electron microscope (TEM) is one of the most powerful imaging instruments. Currently, the TEM enables imaging of three-dimensional (3D) structures on the atomic scale. However, the temporal resolution of TEM is limited by the video-camera recording rate (millisecond), as continuous electron beams produced by DC-acceleration-based thermionic or field-emission sources are used in conventional TEMs. In order to overcome this millisecond temporal resolution limit in TEM, in 1987, Bostanjoglo et al. [1, 2] proposed a technique with a nanosecond-triggered beam-blanking unit in TEM to produce electron beam flashes and succeeded in observation of laser-induced phase transitions in amorphous Ge films with a nanosecond resolution. Two years later, they developed time-resolved electron microscopy with a laser-triggered photoemission electron gun [3, 4] and paved the way for studies and imaging of fast dynamic events with pulsed electron beams. In the time-resolved electron microscopy (pump-probe technique), an initialing pump laser pulse excites the materials (sample) to produce a transient state, and then a later analytical probe electron pulse detects it at a correlated time with the pump pulse, as shown in **Figure 1**. It is worth noting that the temporal resolution is determined by the durations of the pump laser pulse and probe electron pulse. It is

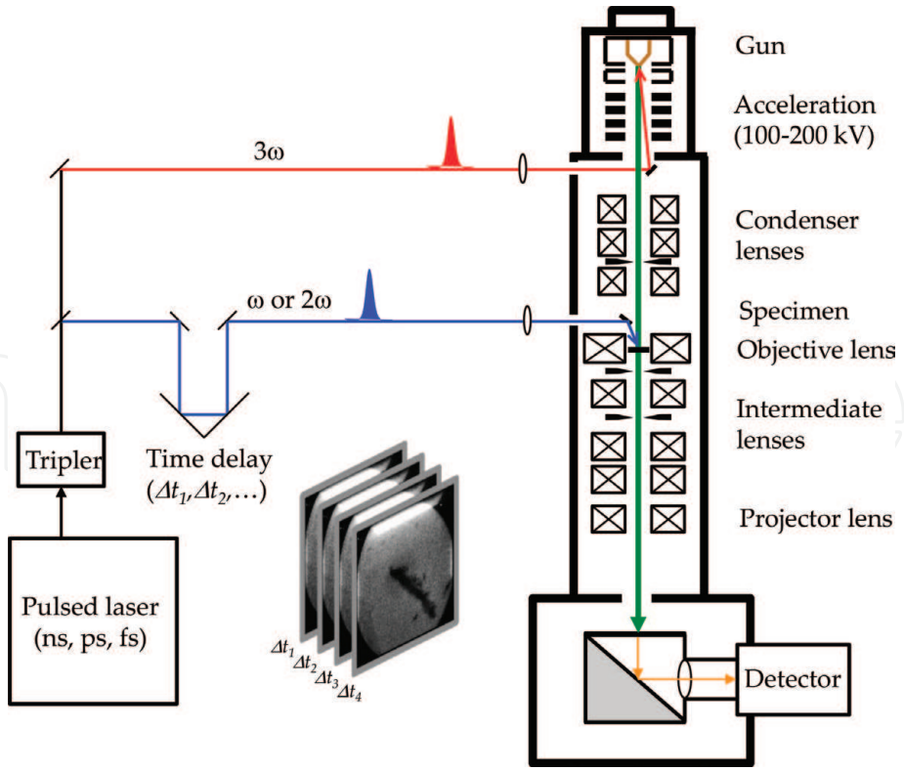

Figure 1.
General schematic of time-resolved electron microscopy using electron pulses.

not limited by the speed of the electron detector. Therefore, the generation of short electron pulses is very significant.

In the past decade, both temporal and spatial resolutions of the time-resolved electron microscopy were improved by several research groups [5–15] by developing high-brightness electron sources and optimizing TEM electron optics. Currently, there are two main approaches to time-resolved electron microscopy: (1) single-shot approach, which uses high-charge electron pulses and (2) stroboscopic approach, which uses "single" electron pulses. The first approach, pioneered by Bostanjoglo et al. (described above), aims to generate a sufficient number of electrons in the pulse to form an image with a single shot. The main advantage of this approach is that the studied structural dynamics or processes do not need to be perfectly reversible. This approach has been developed later at the Lawrence Livermore National Laboratory (LLNL) [5, 6] using a modified JEOL 2000FX for dynamic transmission electron microscopy (DTEM). Single-shot imaging with spatial and temporal resolutions of 10 nm and 15 ns, respectively, has been achieved using a 15-ns electron pulse containing 5×10^7 electrons. DTEM has achieved a spatial resolution of approximately 5 nm and has been applied to various projects, including laser-induced melting of metals, reactions in solid states, and crystallization of amorphous semiconducting materials. However, a serious problem in this approach is the significant space-charge effect due to the Coulomb repulsion of electrons. The high current of the pulses limits the overall temporal and spatial resolutions of the instrument, even with an optimized microscope source, good column, and excellent detector.

The stroboscopic approach uses a femtosecond laser source to generate an extremely low-current electron pulses ("single" electron pulses) at the sample to maintain high temporal and spatial resolutions. A key factor in the stroboscopic approach is to have only a single electron in the column at any time to reduce space-charge effects. Images are constructed from ~10^7 of these single-electron pulses. The first single-electron imaging was demonstrated by Zewail et al. [7–9] at the California Institute of Technology (Caltech) using a modified 120-kV TEM as

a first-generation ultrafast electron microscope (UEM). Later, they constructed a second-generation UEM-2, using a hybrid 200-kV TEM, and achieved spatial and temporal resolutions of 3.4 Å and 250 fs, respectively [8, 9]. The temporal resolution Δt (root-mean-square (RMS)) in UEM is determined by the laser pulse width Δt_{hv} and temporal broadening Δt_{KE} due to excess energy of electrons emitted from the photocathode. It can be calculated as [9]

$$\Delta t = \sqrt{\Delta t_{hv}^2 + \Delta t_{KE}^2}, \tag{1}$$

$$\Delta t_{KE} = \frac{d}{eV}\sqrt{\frac{m_0}{2}}\frac{\Delta E_i}{\sqrt{E_i}}, \tag{2}$$

where e is the electron charge, m_0 is the electron rest mass, ΔE_i is the energy spread of electrons emitted from the cathode, E_i is the mean energy, and V is the potential across the distance d between the cathode and anode. $\Delta t_{KE} \sim 250$ fs at $\Delta E_i = 0.1$ eV and 650 fs at $\Delta E_i = 0.5$ eV [9]. Recently, there are many research activities [10–15] focused on improving the electron source and electron optics inside the microscope to achieve better temporal and spatial resolutions. However, the current UEM has restrictions: (1) the specimen must be pumped ~10^7 times by the laser, which implies that the studied processes must be perfectly reversible, that is, the sample must heal between pulses; (2) the interval between two pulses needs to be longer than the recovery time of the specimen, thus limiting the repetition frequency of laser excitation; and (3) instrumental instabilities such as specimen drift are inevitable at long exposure times. Therefore, for most experiments under realistic conditions, it is necessary to operate with a larger number of electrons per pulse.

All of the current DTEMs and UEMs use a DC-acceleration-based photoemission electron gun to generate electron pulses at energies of 100–200 keV. For such low-energy electron pulses (nonrelativistic electron pulses), the space-charge effect due to the Coulomb repulsion of electrons is a serious problem. It not only broadens the pulse duration but also increases the energy spread and beam divergence during the acceleration (particularly near the cathode) and propagation to the specimen. We can reduce the space-charge broadening in the propagation with a high-energy electron beam, that is, with the use of ultrahigh-voltage electron microscopy. However, the space-charge effect near the cathode can be reduced only by instantaneously accelerating the electrons to high energies with a high electric field. This is very difficult or impossible, as the maximum static electric field in the DC gun is determined by the vacuum breakdown limit of ~10 MV/m. The current state-of-the-art DC guns have been developed to generate 600-fs electron pulses with up to 10,000 electrons per pulse [16]. An approach of electron pulse compression based on the radio frequency (RF) technology was proposed to control the space-charge effect and generate high-current femtosecond electron pulses at the sample position [17–20]. However, this approach is not suitable for microscopy, because of the relatively large energy spread of the electron pulses. From the theoretical modeling and experimental study, it is obvious that it is impossible to use the DC electron gun parameters to attain femtosecond or picosecond electron pulses at the sample position with a reasonable electron number of 10^7 (or larger) for the single-shot imaging.

Recently, an advanced accelerator technology of RF-acceleration-based photoemission electron guns has been successfully applied for ultrafast electron diffraction (UED) with a single-shot measurement [21–30]. The RF gun is usually operated with a high RF electric field equal to or higher than 100 MV/m, which is 10 times higher than those of the DC guns. Therefore, the electrons emitted from the photocathode can be quickly accelerated into the relativistic-energy region to

minimize the space-charge effects in the pulse, yielding a femtosecond or picosecond pulse containing a large number of electrons. Yang et al. have developed the first prototype of relativistic UEM using the RF gun technology at the Osaka University, have succeeded in generation of high-brightness relativistic electron pulses with a pulse duration of 100 fs containing 10^7 electrons at an energy of 3 MeV [31, 32], and have demonstrated the first single-shot imaging using such femtosecond electron pulses [33–36]. This promising approach has a large potential to study ultrafast dynamics in materials, as there are several crucial advantages over nonrelativistic UEM systems:

- The relativistic energy reduces the space-charge effect, which consequently maintains the temporal confinement and beam brightness during the propagation to the sample. It is possible to perform single-shot imaging with femtosecond temporal resolution to observe reversible and irreversible processes in materials.

- Relativistic-energy electrons significantly enhance the extinction distance for elastic scattering and provide structural information, essentially free from multiple scattering and inelastic effects [37]. Our previous UED study of structural dynamics of laser-irradiated gold nanofilms indicates that the kinematic theory can be applied in the case of 3-MeV probe electrons with the assumption of single scattering events [29, 30]. This enables to easily understand and explain structural dynamics.

- A thick sample can be used for measurement, thereby obviating the requirement to prepare suitable thin samples. The utilization of the relativistic electron pulse overcomes the loss of temporal resolution due to the velocity mismatch in samples. Furthermore, the relativistic UEM is suitable for in situ observations as there are large area and space inside the objective lens to install various specimens.

In this chapter, we introduce a UEM with relativistic femtosecond electron pulses, including information of an RF photoemission gun, concept of relativistic UEM, and demonstration experiments with relativistic femtosecond electron pulses.

2. Relativistic UEM

The relativistic UEM consists of a 1.6-cell S-band (2.856 GHz) photocathode RF gun and microscopy column including an electron illumination system, objective lens, and imaging system. **Figure 2** shows a prototype of relativistic UEM, which has a height of 3 m and diameter of 0.7 m.

2.1 Photocathode RF gun

Photocathode RF gun is a high-brightness electron source in the particle accelerator field, which has been widely applied in free-electron lasers [38, 39], and is considered for use in the next linear colliders [40, 41]. The RF gun used in our relativistic UEM consists of two RF cavities: a half cell and full cell. The accelerating RF is 2.856 GHz, belonging to the so-called S-band corresponding to a wavelength of λ = 104.969 mm. The length of the full-cell cavity is $\lambda/2$ = 52.4845 mm, while the length of the half-cell is 31.49 mm, equal to 0.6 times $\lambda/2$, as numerical studies

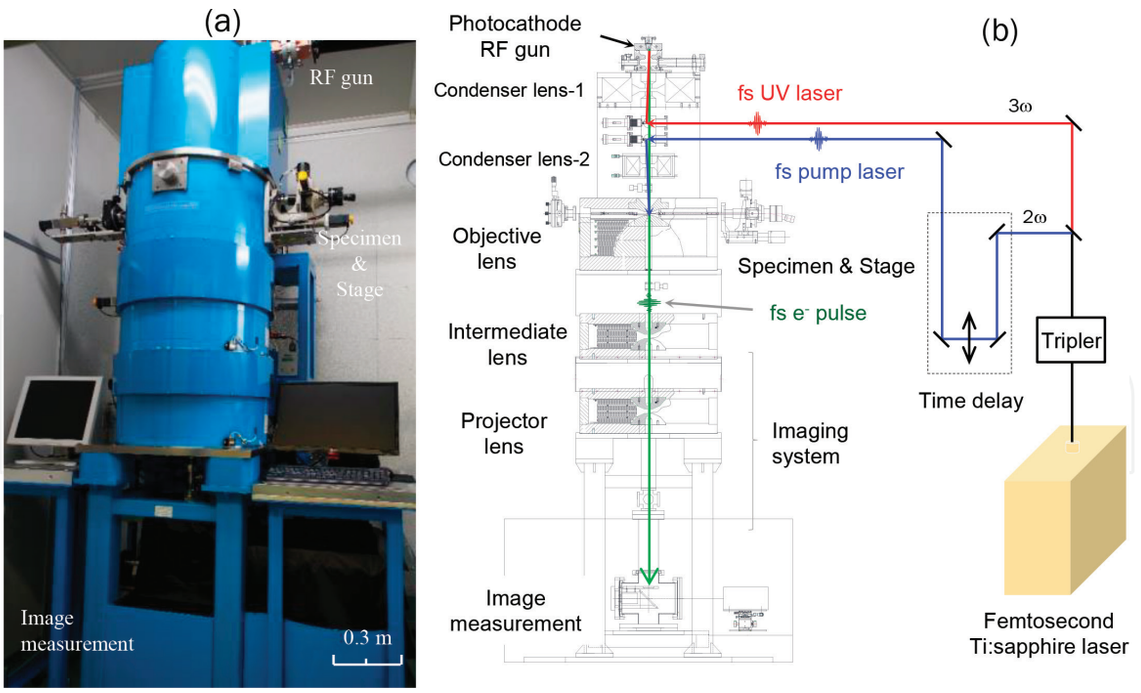

Figure 2.
(a) Photograph and (b) conceptual design of a relativistic UEM with femtosecond electron pulses.

show that more optimal performances are obtained if the half-cell cavity length is 0.6 (rather than 0.5) times the full-cell length. The cross section of the actual RF cavities is shown in **Figure 3(b)**. The shapes of the cavities are optimized to reduce both RF-induced emittance and energy spread. The cavities and other components are carefully fabricated and brazed together to minimize the dark current due to the field emission. A very fine copper photocathode is located at a position of a high-accelerating RF field in the half-cell cavity and is illuminated by the third harmonic of a Ti:sapphire laser (ultraviolet (UV) emission: 266 nm, pulse duration: 100 fs). When the electrons leave the cathode, they are accelerated by a negative electric field in the cavity, as shown in **Figure 3(a)**.

Generally, the RF gun uses the TM_{010} transverse magnetic mode with a phase shift of π between the half cell and full cell. The linear components of the electric and magnetic fields in the RF cavities can be assumed to be [42, 43]

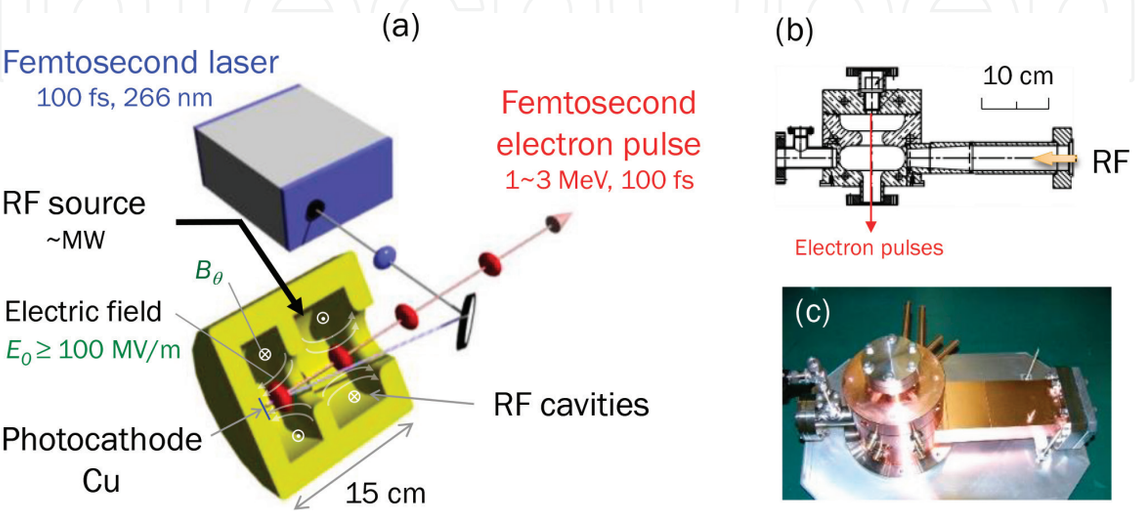

Figure 3.
(a) Schematic of femtosecond electron pulse generation in the photocathode RF gun, (b) the cross section of the RF cavities, and (c) photograph of the RF gun.

$$\begin{aligned} E_z &= E_0 \cos kz \sin(\omega t + \phi_0) \text{ at } r = 0, \\ E_r &= \frac{kr}{2} E_0 \sin kz \sin(\omega t + \phi_0), \\ B_\theta &= c\frac{kr}{2} E_0 \cos kz \cos(\omega t + \phi_0), \end{aligned} \tag{3}$$

where $E_0 \geq 100$ MV/m is the peak accelerating field, $k = 2\pi/\lambda$, $\omega = ck$, c is the velocity of light, and ϕ_0 is the initial RF phase when the electron leaves the cathode surface ($z = 0$) at $t = 0$. For short electron pulses with Gaussian distributions in longitudinal and transverse directions, Kim [42] and Travier [44] reported analytical expressions for the following parameters at the gun exit in practical units: electron energy E in MeV, RMS relative energy spread $\Delta E/E$, RMS angular divergence σ'_x in mrad, normalized RMS RF-induced emittance ε_{rf}, and normalized RMS space-charge-induced emittance ε_{sc} in mm-mrad:

$$E = 75(n + 0.5)\frac{E_0}{f}, \tag{4}$$

$$\frac{\Delta E}{E} = 2 \times 10^{-6} \frac{f\sigma_b}{n + 0.5}, \tag{5}$$

$$\sigma'_x = 0.511 \frac{E_0 \sigma_x}{E + 0.511}, \tag{6}$$

$$\varepsilon_{rf} = 2.73 \times 10^{-11} E_0 f^2 \sigma_x^2 \sigma_b^2, \tag{7}$$

$$\varepsilon_{sc} = 3.76 \times 10^3 \frac{Q}{E_0(2\sigma_x + \sigma_b)}, \tag{8}$$

where E_0 is the peak accelerating field in MV/m, f is the RF in MHz, n is the number of full-cell cavities, Q is the electron charge of the pulse in nC, and σ_b and σ_x are the RMS pulse duration in ps and RMS transverse beam size in mm, respectively, which are dependent on the laser pulse width and spot size on the cathode. These expressions are useful to estimate the beam parameters for the consideration and design of a new RF gun in other instruments. For example, for a 1.5-cell S-band RF gun at $E_0 = 100$ MV/m with a 100-fs and 0.1-mm laser, we estimate the following beam parameters: $E = 3.9$ MeV, $\Delta E/E = 3.8 \times 10^{-4}$, $\sigma'_x = 1.1$ mrad, $\varepsilon_{rf} = 2.2 \times 10^{-6}$ mm-mrad, and $\varepsilon_{sc} = 1.3 \times 10^{-2}$ mm-mrad at $Q = 0.1$ pC. These estimated parameters are in agreement with a particle simulation with the space-charge effect, as described below.

For a short electron pulse with a small beam size, the RF-induced emittance is negligible in the RF gun. In this case, the thermal emittance (initial emittance) at the cathode is dominant. Assuming an isotropic emission into a half sphere in front of the cathode surface, the thermal emittance can be expressed in terms of the RMS incident laser spot size on the cathode σ_r and a kinetic energy of the emitted electrons E_{kin}:

$$\varepsilon_{th} = \sigma_r \sqrt{\frac{2E_{kin}}{3m_0c^2}}, \tag{9}$$

$$E_{kin} = h\upsilon - \varphi + \varphi_{schottky}, \tag{10}$$

$$\varphi_{schottky} = \alpha\sqrt{\beta E_0 \sin\varphi_0}, \tag{11}$$

where $h\nu$ s the laser photon energy, φ is the work function of the cathode, $\phi_{schottky}$ is the reduction in the potential wall barrier due to the Schottky effect, and α and β are a constant and field-enhancement parameter, respectively, which are determined by the roughness and clearness of the cathode surface. Finally, the total beam emittance is

$$\varepsilon = \sqrt{\varepsilon_{rf}^2 + \varepsilon_{sc}^2 + \varepsilon_{th}^2}. \tag{12}$$

For a very fine copper photocathode with a 266-nm laser under the conditions of E_0 = 100 MV/m and ϕ_0 = 30°, the measured thermal emittance exhibited a linear relationship with the RMS laser spot size: ε_{th} [mm-mrad] = 0.74 × σ_r [mm] [45], yielding an E_{kin} = 0.42 eV.

In electron microscopy, the electron gun is required to generate a low-emittance and low-energy-spread beam (normalized emittance ≤0.1 mm-mrad, energy spread ≤10^{-4}). The beam dynamics in the RF gun can be calculated by a theoretical simulation using the General Particle Tracer (GPT) code [46]. **Figure 4** presents the simulation results of relativistic femtosecond-pulsed electron beams at the specimen position in the UEM generated from a 1.6-cell S-band RF gun. The results of the beam dynamics show that (1) the minimum energy spread is obtained at the launch phase of approximately 20°. At $\phi_0 \geq 60°$, the energies of the electrons decrease leading to the large increases in the energy spread due to the space-charge effects during the electron propagation. The slight increase in the energy spread

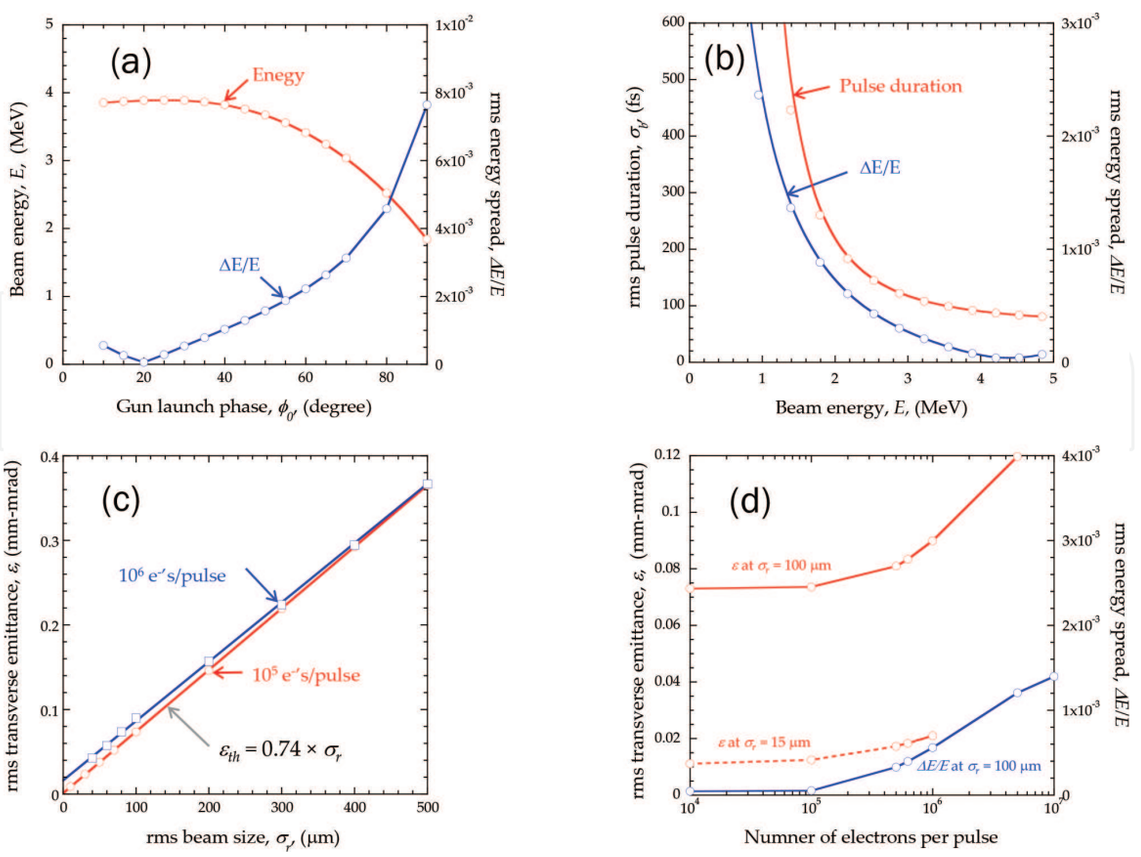

Figure 4.
Simulation results of the beam energy, pulse duration, emittance, and energy spread of electron pulses generated by the RF gun driven with a 100-fs laser under the conditions of (a) Q = 0.16 pC and E_0 = 100 MV/m, (b) Q = 0.16 pC and ϕ_0 = 20°, (c) E = 3.8 MeV and ϕ_0 = 20°, and (d) E = 3.8 MeV and ϕ_0 = 20°.

at $\phi_0 < 20°$ is caused by the space-charge effect near the cathode as the actual RF electric field is decreased by $E_0 \sin\phi_0$, (2) large increases in both energy spread and pulse duration are observed at an electron energy smaller than 3 MeV, and (3) the transverse emittance of the femtosecond electron pulses generated from the RF gun is dominated mainly by the thermal emittance if the number of electrons in the pulse is 10^6 (or smaller). This allows us to generate low-emittance electron pulses by focusing the laser spot on the cathode, as described in Eq. (9). The increase in the energy spread due to the space-charge effect is also negligible at an electron number smaller than or equal to 10^6 per pulse. The theoretical modeling and particle simulation indicate that the RF gun could generate high-current femtosecond electron pulses with excellent characteristics, including a normalized RMS transverse emittance of 0.02 mm-mrad, energy spread of 10^{-4} to 10^{-5}, and pulse duration of 100 fs with 10^6 electrons per pulse at an energy larger than or equal to 3 MeV. The peak brightness of such electron pulses B_p can be calculated by

$$B_p = (\beta\gamma)^2 \frac{Q}{\varepsilon^2 \sigma_b}, \tag{13}$$

where $\beta = v/c$, v is the electron velocity, and γ is the normalized relativistic energy. From the given parameters, we can calculate the peak brightness, $B_p = 2 \times 10^{17}$ A/m^2·sr. Recently, the development of a high-repetition-rate normal-conducting RF gun at 1000 Hz was proposed in our research group. In the near future using this RF gun, the time-averaged brightness of the femtosecond-pulsed electron beam can be potentially increased to $B = 2 \times 10^7$ A/m^2·sr, corresponding to the brightness of the 100-kV thermionic emission gun used in modern TEMs. In addition, if we can further reduce the energy spread, the RF gun will pave the way for generation of a practical high-brightness femtosecond-pulsed electron beam for UEM.

2.2 UEM column

2.2.1 Electron illumination system

The electron illumination system comprises two condenser lenses and condenser aperture to control and transfer the electron pulses from the RF gun on the specimen, as shown in **Figure 5**. An aperture with three pinholes with diameters of 0.5, 1, and 2 mm is made of a 1-mm-thick molybdenum metal and is installed between the two condenser lenses. The distance from the photocathode to the specimen is 0.8 m. However, there are two significant differences from the normal TEMs: (1) there is no gun crossover in the RF gun and (2) we cannot produce a crossover between the two condenser lenses owing to the space-charge effect (i.e., the condenser lenses do not condense). Therefore, in this illumination system, the image of the beam spot on the cathode acts as the object plane of the first condenser lens as the beam size is minimum in the RF gun. It is worth noting that a virtual source image behind the cathode may be better for the object plane of the first lens as the source size is smaller than that on the cathode, as shown in **Figure 5**. We adjust the first lens to create a parallel electron beam. The aperture stops the large-divergence electrons to further reduce the emittance, yielding a small illumination convergence angle at the specimen. Finally, we used the second lens to create a parallel beam or convergent beam on the specimen. The parallel beam is used primarily for UEM imaging and selected-area diffraction (SAD), while the convergent beam is used mainly for convergent-beam electron diffraction (CBED). In the experiments, a small convergence angle of $\alpha = 31$ μrad was achieved with the condenser aperture with the pinhole diameter of 0.5 mm in the parallel-beam operation mode.

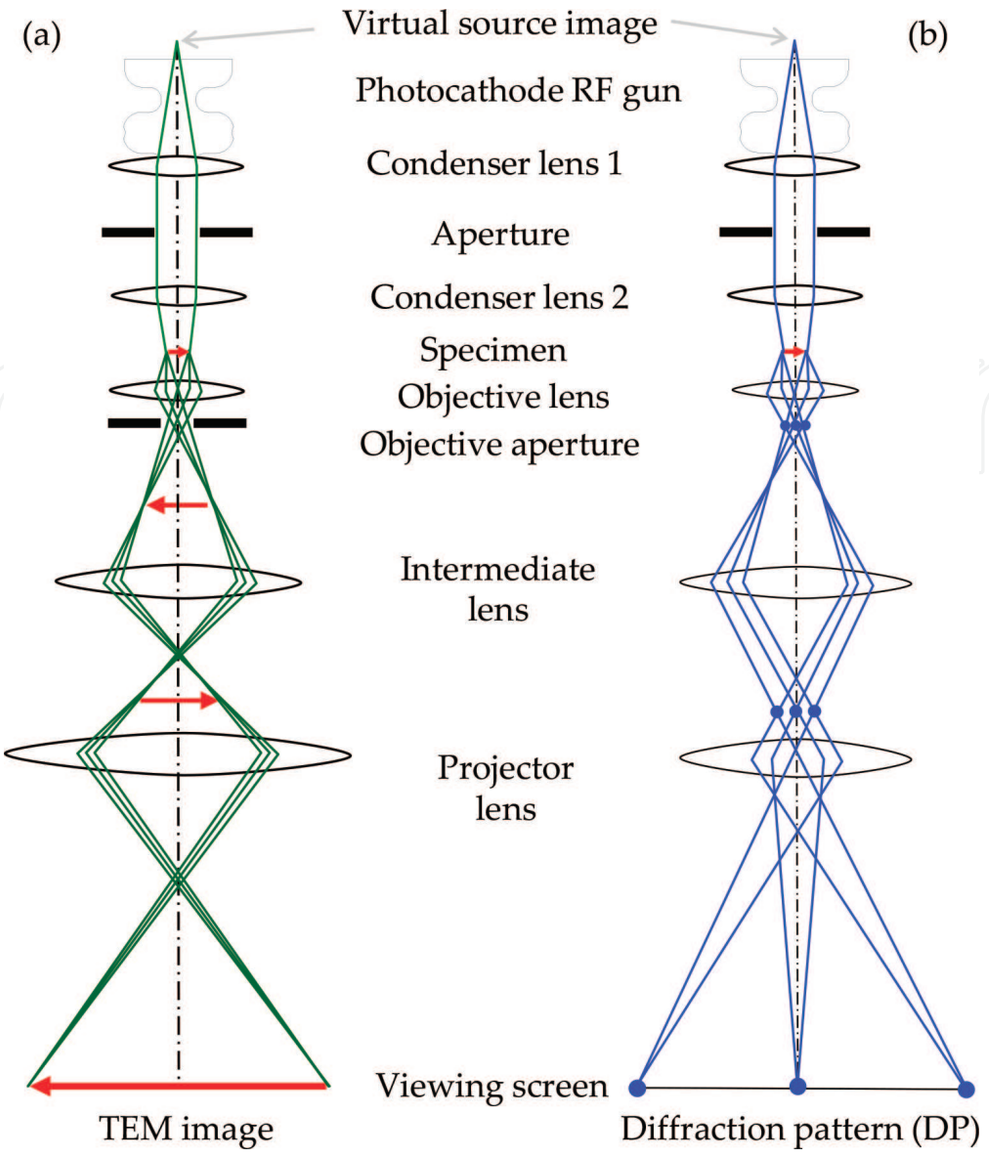

Figure 5.
Two basic operations of the UEM imaging system: (a) imaging mode: Projection of a TEM image onto the viewing screen and (b) diffraction mode: Projection of diffraction patterns (DPs) onto the screen.

2.2.2 Objective lens

The objective lens is the most important lens in a TEM. It forms TEM images or DPs, magnified by the other lenses. It is very challenging to construct this lens as the specimen must be located close to its center. In the UEM, two asymmetrical and separable pole pieces (upper and lower) are used for the objective lens. The gap between the pole pieces is 19 mm. It allows us to insert both specimen and aperture between the pole pieces. With the large gap, it is straightforward to design specimen holders for various tasks such as tilting, rotation, heating, cooling, straining, etc. The gap-to-bore ratio is 1.46 for creation of a strong magnetic field and aberration suppression. We carefully designed and produced all of the pole pieces, iron circuits, coils, and water-cooling components. The pole pieces were made of a soft magnetic alloy (Permendur) with an iron-to-cobalt content ratio of 1:1. The saturation magnetic flux density is 2.4 T. The objective lens is a very strong lens. The maximum magnetic field strength at the center of the pole pieces is 2.3 T under the magnetomotive force of 35 kA·turns. The focal length is 5.8 mm for a 3-MeV electron beam. The diameter of the lens is 0.7 m, as shown in **Figure 6(a)**.

The specimen is placed close to the center of the pole pieces with a side-entry method and manipulated by a five-axis motorized stage. The sample can be pumped by a pulsed laser beam, as shown in **Figure 2**. An objective aperture with a pinhole diameter of 0.3 mm is inserted at the back-focal plane of the objective lens to block scattered electrons in the imaging operation mode.

2.2.3 Imaging system

The imaging system uses two magnetic lenses (intermediate and projector lenses) to magnify the TEM image or DP produced by the objective lens and to project it onto a viewing screen (scintillator) through a charge-coupled device (CCD) camera. In the intermediate and projector lenses, two symmetrical and separable pole pieces are used. The gap is 20.8 mm, while the gap-to-bore ratio is ~1.6 for minimization of the aberration coefficients. The pole pieces in the intermediate and projector lenses are made of Permendur and pure iron, respectively. The distance between the objective and intermediate lenses is 0.6 m. The distance between the intermediate and projector lenses is ~0.4 m. The maximum magnetic field strengths are 2.3 T in the intermediate lens and 1.2 T in the projector lens.

In a time-resolved image measurement with the pump-probe technique, the spread of the detector (recording rate of the video-camera) does not limit the temporal resolution; however, a high-sensitivity detection of electron waves is crucial. In particular, acquisition of images in a single shot is necessary in order to observe irreversible processes. In addition, as mentioned above, the space-charge effect causes increases in the pulse duration, emittance, and energy spread, even in relativistic electron beams. Low-current electron pulses should be used in the UEM. Therefore, the image recording system should be highly sensitive to every electron. In the UEM, in order to achieve a high sensitivity to MeV electron detection with a high damage threshold, we chose a Tl-doped CsI columnar crystal scintillator equipped with a fiber optic plate (Hamamatsu Photonics) to convert the relativistic-energy TEM images or DPs into optical images. The light generated by the scintillator is propagated by a reflective mirror (at 45°) consisting of aluminum deposited on a 5-μm-thick polymer, and finally the optical images are detected with an electron-multiplying CCD (EMCCD) with 1024 × 1024 pixels, as shown in **Figure 6(b)**. The effective detection area of the scintillator is 50 × 50 mm^2, while the distance from the specimen to the scintillator is 1.8 m. The sensitivity of the whole detection system is 3 × 10^{-3} counts/electron.

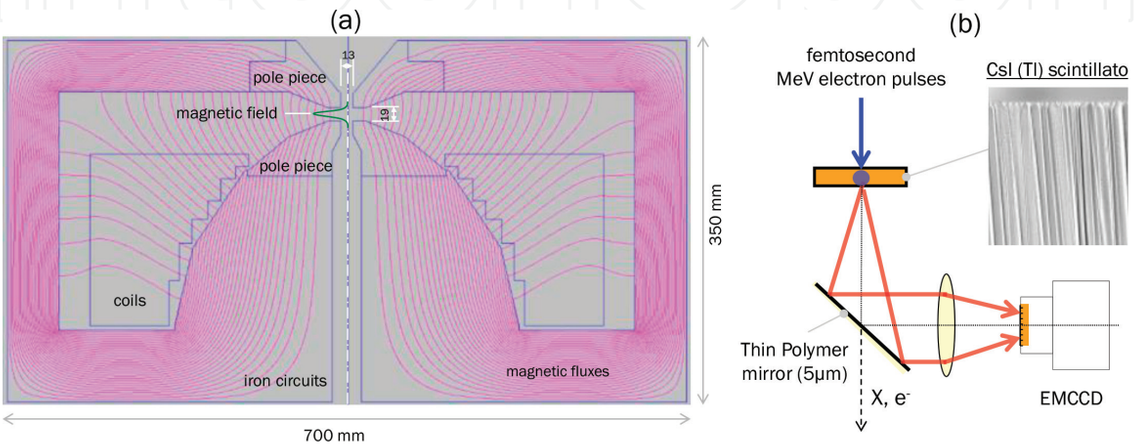

Figure 6.
(a) Cross section of the objective lens and (b) image detection system with a CsI (Tl) scintillator.

2.3 Femtosecond laser system

A femtosecond Ti:sapphire laser (Spectra-Physics) is used to generate femtosecond electron beam pulses and to excite the specimen. The laser consists of a Ti:sapphire laser oscillator with a pulse width of 90 fs (Tsunami, central wavelength: 800 nm), regenerative amplifier including a pulse compressor, and a wavelength converter. The femtosecond laser oscillator is synchronized to a 79.3-MHz RF signal, corresponding to 1/36 of the 2856-MHz RF used for the electron generation in the RF gun, with a time-to-lock piezoelectric device. The time jitter between the laser pulse and RF phase is 61 fs [36]. The laser pulses generated from the oscillator are fed to the regenerative amplifier and amplified to ~1 mJ per pulse. The regenerative amplifier is driven by a green laser with a highly stable repetition rate of 1 kHz (Empower, wavelength: 532 nm, output: 10 W).

The amplified femtosecond pulses are converted to the third harmonics by a wavelength converter (Tripler) composed of two nonlinear crystals (SHG and THG) and time plate for pulse delay adjustment. The third-harmonic pulses (UV wavelength: 266 nm) with the maximum energy of 70 μJ per pulse are illuminated onto the copper cathode to generate femtosecond electron pulses. The residual fundamental (wavelength: 800 nm) and second-harmonic (wavelength: 400 nm) pulses are used to pump the samples. The time delay between the pump laser pulse and probe electron pulse is changed with an optical delay located on the pump laser beam line for time-resolved experiments. Both laser beams used for the electron generation and sample excitation can be focused to a spot size with a full width at half maximum (FWHM) smaller than 30 μm at the corresponding target.

3. Observations with relativistic femtosecond electron pulses

3.1 UEM (imaging mode)

In the imaging operation mode of the relativistic UEM, we adjust the intermediate lens so that its object plane is the image plane of the objective lens and then project the image onto the scintillator with the projection lens, as shown in **Figure 5(a)**. The objective aperture with a pinhole diameter of 0.3 mm inserted at the back-focal plane of the objective lens is used to block the diffraction patterns and other scattered electrons.

Figure 7 shows bright-field UEM images of polystyrene latex particles, with diameters of 1.09 μm and gold nanoparticles with diameters of 400 ± 20 nm, dispersed on a carbon film pasted on a copper mesh, observed with a pulse integration measurement [35]. The magnification of the images is approximately 1500×. The energy of the electron pulses used for the observations is 3.1 MeV. The pulse duration is approximately 100 fs. In this experiment, a condenser aperture with a pinhole diameter of 0.5 mm is used to collimate the electron beam. The repetition rate of the electron pulses is 10 Hz. The normalized RMS emittance and electron charge in the pulses are 0.12 mm-mrad and 1 pC at the specimen position, respectively. From these parameters, the estimated peak brightness of the pulses in the observations is $B_p = 3.5 \times 10^{16}$ A/m^2·sr. For these electron pulses, acceptable images of both polystyrene latex particles and gold nanoparticles can be obtained using our relativistic UEM with 2000- and 500-pulse integrations, respectively.

At a low-magnification observation condition, the single-shot observation of UEM images with a relativistic femtosecond electron pulse is achievable. **Figure 8** presents UEM images of single-crystal gold obtained with a single shot and 10- and

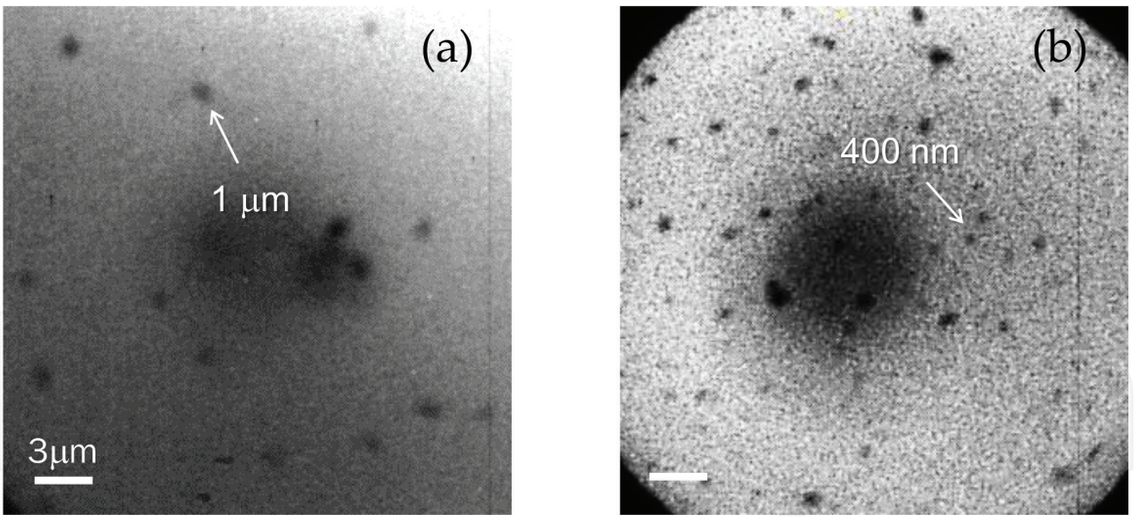

Figure 7.
UEM images (bright field) of (a) polystyrene latex particles with a diameter of 1.09 μm and (b) gold nanoparticles with a diameter of 400 ± 20 nm obtained by 2000 and 500-pulse integrations, respectively, with 100-fs electron pulses at an energy of 3.1 MeV [35].

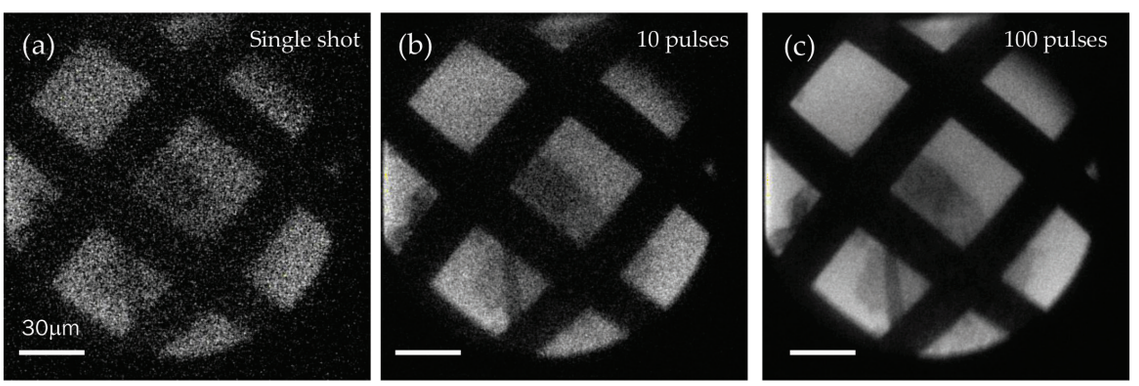

Figure 8.
UEM images (bright field) of gold single-crystals placed on a gold mesh observed by (a) a single shot and (b) 10- and (c) 100-pulse integrations with 100-fs electron pulses at an energy of 3.1 MeV.

100-pulse integrations. The sample is a single-crystalline gold film with a thickness of 10 nm placed on a gold mesh. Although the signal-to-noise ratio is still not sufficient in the single shot, an acceptable image can be obtained with 10 pulses (or more), as shown in **Figure 8(b)** and **(c)**. This demonstrates that the single-shot observation of UEM images with a relativistic electron pulse is achievable if the brightness of the pulses can be increased by one order of magnitude, $B_p \sim 10^{17}$ A/m^2·sr, which can be realized, as described in Section 2.1.

3.2 UED (diffraction mode)

In the relativistic-energy electron diffraction measurement (diffraction mode), we adjust the imaging-system lenses so that the back-focal plane of the objective lens acts, as the object plane for the intermediate lens, and then use the projection lens to project the DPs onto the scintillator, as shown in **Figure 5(b)**. It is worth noting that in the diffraction mode, if the electron beam is too intense, it will damage the viewing screen or saturate the CCD camera. Therefore, we could generate a smaller beam to reduce the illuminated area of the specimen contributing to the DP on the screen. The use of a selected-area aperture inserted at the image plane of the objective lens is a better choice to create a virtual aperture in the plane of the specimen, thus yielding only the SAD pattern. In the diffraction mode, the objective aperture is not used.

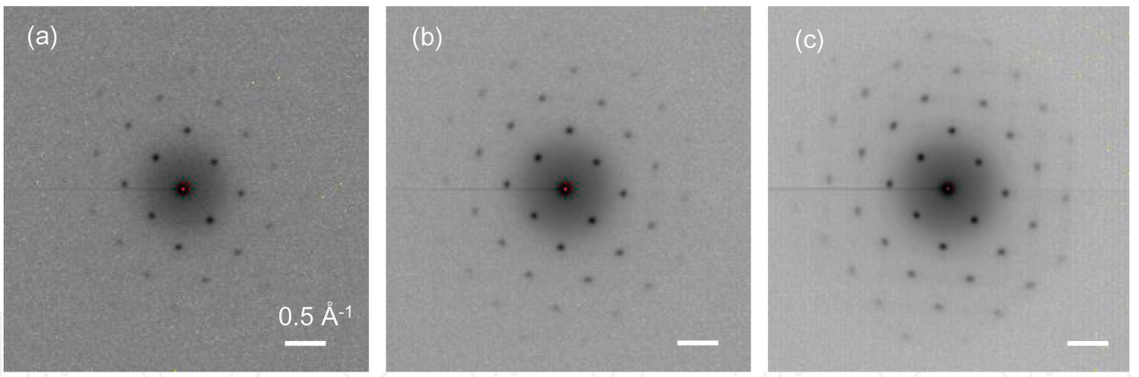

Figure 9.
DPs of a (100)-oriented single-crystalline gold measured with (a) a single shot and (b) 10- and (c) 100-pulse integrations. The energy of the electron pulses is 3.1 MeV, while the number of electrons in each pulse is 6.3×10^6, corresponding to 1 pC per pulse.

In order to check the contrast of the DPs and resolution, we generate a parallel electron beam with a diameter of 0.5 mm to illuminate the specimen using a condenser aperture with a diameter of 0.5 mm and weakened second condenser lens in the illumination system. The characteristics of the electron pulses are the same as those in the imaging operation mode. **Figure 9** presents the DPs of the single-crystal gold observed by a single shot and 10- and 100-pulse integrations. The sample is a single-crystalline gold film with a thickness of 10 nm placed on a gold mesh. The energy of the electron pulses is 3.1 MeV. The electron charge per pulse is 1 pC. Data in **Figure 9** show that (1) sharp DPs and high contrast can be obtained with the relativistic femtosecond electron pulses, (2) higher order spots of (−420) and (4–20) from the single-crystal gold with scattering vectors up to 1.1 $Å^{-1}$ can be clearly captured with a single shot, and (3) the RMS width of the zeroth-order spot (000) in the single shot is measured to be 0.018 $Å^{-1}$, indicating an excellent spatial resolution for the relativistic diffracted beam.

Based on the width of the (000) spot and measured distance of the diffraction spots from the (000) position, the estimated RMS illumination convergence angle α of the electron beam at the specimen is α = 31 μrad. This convergence angle is two orders of magnitude smaller than that of nonrelativistic UED. Additionally, the coherence of the electron source is an important parameter in diffraction imaging, particularly in terms of spatial coherence (transverse coherence), which determines the sharpness of the DPs and diffraction contrast in the acquired images. The spatial coherence length is defined as

$$d_c = \frac{\lambda_e}{2\alpha}, \tag{14}$$

where λ_e is the electron wavelength and α is the RMS illumination convergence angle. Using the obtained illumination convergence angle, the spatial coherence length of the electron pulses generated with the RF gun is d_c = 5.6 nm, twice that of the current UED systems. This enables to detect sharp DPs and acquire good-contrast diffraction images with a single shot, as shown in **Figure 9**.

The temporal resolution can be characterized in the time-resolved electron diffraction studies. **Figure 10** presents an example of time-resolved experiment for observation of UED structural dynamics in a 35-nm thick single-crystalline silicon sample. The sample was pumped by a 400-nm laser beam with a pulse duration of 100 fs and density of 3.5 mJ/cm^2. The UED patterns were measured with a single shot using a 3-MeV electron pulse with the pulse duration of 100 fs containing 10^5 electrons per pulse. The data elucidate the dynamics in the silicon crystals: the

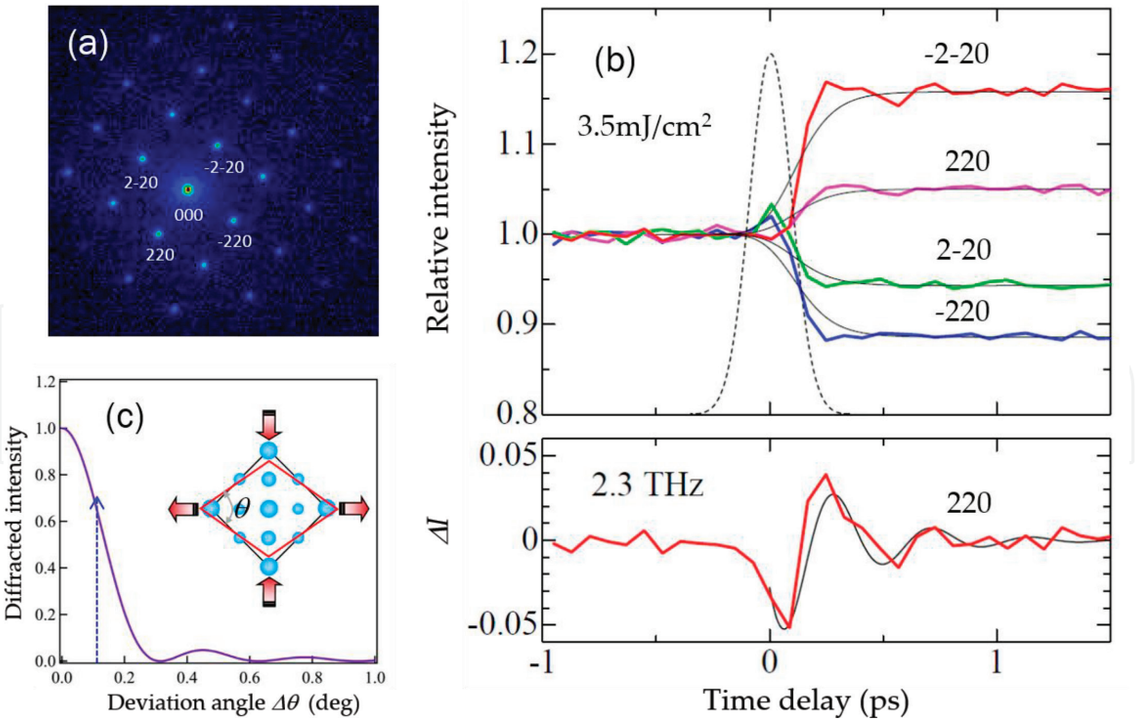

Figure 10.
UED structural dynamics. (a) DPs of a (100)-oriented single-crystalline silicon with a thickness of 35 nm measured by a 3-MeV femtosecond electron pulse with a single shot. The pusle duration of the electron pulse is ~ 100 fs containing 10^5 electrons. (b) Intensity changes for four Bragg spots after the laser illumination. The wavelength and density of the pump femtosecond laser are 400 nm and 3.5 mJ/cm2, respectively. (c) Simulation results of diffracted intensity changes due to lattice distortion within a angle of $\Delta\theta < 0.1°$ along the (111)-oriented direction [47].

diffracted intensities of the Bragg spots along the (−2–20) and (220) line increase, while the intensities of the Bragg spots along the (2–20) and (−220) line decrease after the laser pump. The structural recovery after a change is very slow. Tanimura and Naruse [47] suggested that these dynamics are caused mainly by the lattice distortion due to the laser excitation in silicon crystals, indicating that the time-resolved diffraction methodology in the relativistic UEM could be utilized to obtain an atomic perspective of lattice motion in crystalline materials.

The total temporal resolution of the UEM can be estimated mainly with the probe electron pulse duration σ_b, pump laser pulse width σ_b, and time jitter Δt_j between two pulses as

$$\Delta t = \sqrt{\sigma_b^2 + \sigma_l^2 + \Delta t_j^2}. \quad (15)$$

The time jitter is determined by the synchronization of the laser pulse to the accelerating RF phase; therefore, we can define Δt_j = 61 fs, described in Section 2.3. In our relativistic UEM, both pump and probe pulse durations are ~ 100 fs (RMS). The estimated total temporal resolution is approximately 150 fs (RMS), corresponding to the experimental results represented by the dashed line in **Figure 10(b)**.

4. Conclusions

In this chapter, we have introduced a relativistic UEM with femtosecond electron pulses, including the relativistic femtosecond electron pulse generation with an RF-acceleration-based photoemission gun, first prototype relativistic UEM instrument, and demonstrations of UEM image and UED measurements with the

relativistic femtosecond electron pulses. The electron pulses generated by the RF gun exhibited excellent characteristics, including a low emittance of ≤0.1 mm-nrad, energy spread of 10^{-4}, and pulse duration of 100 fs with 10^6 electrons per pulse at an energy ≥3 MeV. These pulses have facilitated (1) the acquisition of high-quality high-resolution diffraction patterns with a single shot, (2) acquisition of acceptable UEM images with pulse integration measurements, and (3) time-resolved experiments with an excellent temporal resolution of 150 fs, suggesting that the relativistic UEM is very promising for studies on ultrafast phenomena in the femtosecond time region.

Ultrahigh-voltage electron microscopes operated in the relativistic-energy region above 1 MeV have attracted significant attention in various research fields, including physics, biology, and materials science. However, the existing system is too large and expensive to be purchased and operated even by large-scale facilities such as universities or national research centers, not to mention smaller research institutions and laboratories. The RF electron gun is capable of acceleration to ≥3 MeV in a length of only 15 cm. Further reductions in the emittance and energy spread, increase in the repetition rate, and suppression of some instabilities are required; however, the improvement in the RF gun and resolution refinement to the angstrom level will enable new electron microscopes based on this RF gun, sufficiently small and inexpensive for general research institutions and laboratories. Furthermore, by providing a femtosecond temporal resolution, such relativistic UEMs will constitute the next-generation electron microscopes, referred to as "dream machines," desired for a long time by material-structure researchers throughout the world.

Acknowledgements

The author acknowledges K. Kan, T. Kandoh, M. Gohdo, Y. Yoshida, H. Yasuda, and K. Tanimura of the Osaka University for their valuable suggestions and discussions. Additionally, the author thanks J. Urakawa, T. Takatomi, and N. Terunuma of the High Energy Accelerator Research Organization (KEK) for the design and fabrication of the high-quality RF gun.

This work was supported by a basic research (A) (No. 22246127, No. 26246026, and No. 17H01060) of the Grant-in-Aid for Scientific Research from the MEXT, Japan.

IntechOpen

Author details

Jinfeng Yang
The Institute of Scientific and Industrial Research, Osaka University, Osaka, Japan

*Address all correspondence to: yang@sanken.osaka-u.ac.jp

References

[1] Bostanjoglo O, Tornow RP, Tornow W. Nanosecond-exposure electron microscopy and diffraction. Journal of Physics E: Scientific Instruments. 1987;**20**:556-557. http://iopscience.iop.org/0022-3735/20/5/018

[2] Bostanjoglo O, Tornow RP, Tornow W. Nanosecond-exposure electron microscopy of laser-induced phase transformations. Ultramicroscopy. 1987;**21**:367-372. DOI: 10.1016/0304-3991(87)90034-9

[3] Bostanjoglo O, Heinricht F. A reflection electron microscope for imaging of fast phase transitions on surface. The Review of Scientific Instruments. 1990;**61**:1223-1229. DOI: 10.1063/1.1141952

[4] Bostanjoglo O, Elschner R, Mao Z, Nink T, Weingartner M. Nanosecond electron microscopes. Ultramicroscopy. 2000;**81**:141-147. DOI: 10.1016/S0304-3991(99)00180-1

[5] Kim JS, LaGrange T, Reed BW, Taheri ML, Armstrong MR, King WE, et al. Imaging of transient structures using nanosecond in situ TEM. Science. 2008;**321**:1472-1475. DOI: 10.1126/science.1161517

[6] LaGrange T, Campbell GH, Reed BW, Taheri M, Pesavento JB, Kim JS, et al. Nanosecond time-resolved investigations using the in situ of dynamic transmission electron microscope (DTEM). Ultramicroscopy. 2008;**108**:1441-1449. DOI: 10.1016/j.ultramic.2008.03.013

[7] Barwick B, Park HS, Kwon OH, Baskin JS, Zewail AH. 4D imaging of transient structures and morphologies in ultrafast electron microscopy. Science. 2008;**322**:1227-1231. DOI: 10.1126/science.1164000

[8] Zewail AH. Four-dimensional electron microscopy. Science. 2010;**328**:187-193. DOI: 10.1126/science.1166135

[9] Zewail AH, Thomas JM. 4D Electron Microscopy: Imaging in Space and Time. London: Imperial College Press; 2010. https://doi.org/10.1142/p641

[10] Piazza L, Masiel DJ, LaGrange T, Reed BW, Barwick B, Carbone F. Design and implementation of a fs-resolved transmission electron microscope based on thermionic gun technology. Chemical Physics. 2013;**423**:79-84. DOI: 10.1016/j.chemphys.2013.06.026

[11] Bücker K, Picher M, Crégut O, LaGrange T, Reed BW, Park ST, et al. Electron beam dynamics in an ultrafast transmission electron microscope with Wehnelt electrode. Ultramicroscopy. 2016;**171**:8-18. DOI: 10.1016/j.ultramic.2016.08.014

[12] Feist A, Bach N, Rubiano da Silva N, Danz T, Möller M, Priebe KE, et al. Ultrafast transmission electron microscopy using a laser-driven field emitter: Femtosecond resolution with a high coherence electron beam. Ultramicroscopy. 2017;**176**:63-73. DOI: 10.1016/j.ultramic.2016.12.005

[13] Kuwahara M, Nambo Y, Aoki K, Sameshima K, Jin X, Ujihara T, et al. The Boersch effect in a picosecond pulsed electron beam emitted from a semiconductor photocathode. Applied Physics Letters. 2016;**109**:013108. DOI: 10.1063/1.4955457

[14] Houdellier F, Caruso GM, Weber S, Kociak M, Arbouet A. Development of a high brightness ultrafast transmission electron microscope based on a laser-driven cold field emission source. Ultramicroscopy. 2018;**186**:128-138. DOI: 10.1016/j.ultramic.2017.12.015

[15] Manz S, Casandruc A, Zhang D, Zhong Y, Loch RA, Marx A, et al. Mapping atomic motions with ultrabright electrons: Towards fundamental limits in space-time resolution. Faraday Discussions. 2015;**177**:467-491. DOI: 10.1039/C4FD00204K

[16] Siwick BJ, Dwyer JR, Jordan RE, Dwayne Miller RJ. An atomic-level view of melting using femtosecond electron diffraction. Science. 2003;**302**:1382-1385. DOI: 10.1126/science.1090052

[17] Harb M, Ernstorfer R, Dartigalongue T, Hebeisen CT, Jordan RE, Dwayne Miller RJ. The Journal of Physical Chemistry. B. 2006;**110**:25308-25313. DOI: 10.1021/jp064649n

[18] Van Oudheusden T, de Jong EF, van der Geer SB, Op't Root WPEM, Luiten OJ. Electron source concept for single-shot sub-100 fs electron diffraction in the 100 keV range. Journal of Applied Physics. 2007;**102**:093501. DOI: 10.1063/1.2801027

[19] Sciaini G, Dwayne Miller RJ. Femtosecond electron diffraction: Heralding the era of atomically resolved dynamics. Reports on Progress in Physics. 2011;**74**:096101. DOI: 10.1088/0034-4885/74/9/096101

[20] Van Oudheusden T, Pasmans PLEM, Van der Geer SB, Loos MJD, Van der Wiel MJ, Luiten OJ. Compression of subrelativistic space-charge-dominated electron bunches for single-shot femtosecond electron diffraction. Physical Review Letters. 2010;**105**:264801. DOI: 10.1103/PhysRevLett.105.264801

[21] Hastings JB, Rudakov FM, Dowell DH, Schmerge JF, Cardoza JD, Castro JM, et al. Ultrafast time-resolved electron diffraction with megavolt electron beam. Applied Physics Letters. 2006;**89**:184109. DOI: 10.1063/1.2372697

[22] Li RK, Tang CX, Du YC, Huang WH, Du Q, Shi JR, et al. Experimental demonstration of high quality MeV ultrafast electron diffraction. The Review of Scientific Instruments. 2009;**80**:083303. DOI: 10.1063/1.3194047

[23] Musumeci P, Moody JT, Scoby CM. Relativistic electron diffraction at the UCLA Pegasus photoinjector laboratory. Ultramicroscopy. 2008;**108**:1450-1453. DOI: 10.1016/j.ultramic.2008.03.011

[24] Murooka Y, Naruse N, Sakakihara S, Ishimaru M, Yang J, Tanimura K. Transmission-electron diffraction by MeV electron pulses. Applied Physics Letters. 2011;**98**:251903. DOI: 10.1063/1.3602314

[25] Zhu P, Zhu Y, Hidaka Y, Wu L, Cao J, Berger H, et al. Femtosecond time-resolved MeV electron diffraction. New Journal of Physics. 2015;**17**:063004. DOI: 10.1088/1367-2630/17/6/063004

[26] Harb M, Peng W, Sciaini G, Hebeisen CT, Ernstorfer R, Eriksson MA, et al. Excitation of longitudinal and transverse coherent acoustic phonons in nanometer free-standing films of (001) Si. Physical Review B. 2009;**79**:094301. DOI: 10.1103/PhysRevB.79.094301

[27] Shen X, Li RK, Lundstrom U, Lane TJ, Reid AH, Weathersby SP, et al. Femtosecond mega-electron-volt electron microdiffraction. Ultramicroscopy. 2018;**184**:172-176. DOI: 10.1016/j.ultramic.2017.08.019

[28] Fu F, Liu S, Zhu P, Xiang D, Zhang J, Cao J. High quality single shot ultrafast MeV electron diffraction from a photocathode radio-frequency gun. The Review of Scientific Instruments. 2014;**85**:083701. DOI: 10.1063/1.4892135

[29] Giret Y, Naruse N, Daraszewicz SL, Murooka Y, Yang J, Duffy DM, et al.

Determination of transient atomic structure of laser-excited materials from time-resolved diffraction data. Applied Physics Letters. 2013;**103**:253107. DOI: 10.1063/1.4847695

[30] Daraszewicz SL, Giret Y, Naruse N, Murooka Y, Yang J, Duffy DM, et al. Structural dynamics of laser-irradiated gold nanofilms. Physical Review B. 2013;**88**:184101. DOI: 10.1103/PhysRevB.88.184101

[31] Yang J, Kan K, Naruse N, Yoshida Y, Tanimura K, Urakawa J. 100-femtosecond MeV electron source for ultrafast electron diffraction. Radiation Physics and Chemistry. 2009;**78**:1106-1111. DOI: 10.1016/j.radphyschem.2009.05.009

[32] Kan K, Yang J, Kondoh T, Yoshida Y. Development of femtosecond photocathode RF gun. Nuclear Instruments and Methods A. 2011;**659**:44-48. DOI: 10.1016/j.nima.2011.08.016

[33] Yang J, Yoshida Y, Shibata H. Femtosecond time-resolved electron microscopy. Electronics and Communications in Japan. 2015;**98**:50-57. DOI: 10.1002/ecj.11763

[34] Yang J. Ultrafast electron microscopy using relativistic-energy femtosecond electron pulses. Microscopy. 2015;**156-159**:50 (Japanese). http://microscopy.or.jp/jsm/wp-content/uploads/publication/kenbikyo/50_3/50_3e04jy.html

[35] Yang J, Yoshida Y, Yasuda H. Ultrafast electron microscopy with relativistic femtosecond electron pulses. Microscopy. 2018;in press. DOI: 10.1093/jmicro/dfy032

[36] Yang J, Kan K, Kondoh T, Yoshida Y, Tanimura K, Urakawa J. Femtosecond pulse radiolysis and femtosecond electron diffraction. Nuclear Instruments and Methods A. 2011;**637**:S24-S29. https://doi.org/10.1016/j.nima.2010.02.014

[37] Kurata H, Moriguchi S, Isoda S, Kobayashi T. Attainable resolution of energy-selecting image using high-voltage electron microscope. Journal of Electron Microscopy. 1996;**45**:79-84. DOI: 10.1093/oxfordjournals.jmicro.a023416

[38] Akre R, Dowell D, Emma P, Frisch J, Gilevich S, Hays G, et al. Commissioning the Linac coherent light source injector. Physical Review Accelerators and Beams. 2008;**11**:030703. DOI: 10.1103/PhysRevSTAB.11.030703

[39] Gulliford C, Bartnik A, Bazarov I, Cultrera L, Dobbins J, Dunham B, et al. Demonstration of low emittance in the Cornell energy recovery linac injector prototype. Physical Review Accelerators and Beams. 2013;**16**:073401. DOI: 10.1103/PhysRevSTAB.16.073401

[40] Terunuma N, Murata A, Fukuda M, Hirano K, Kamiya Y, Kii T, et al. Improvement of an S-band RF gun with a Cs_2Te photocathode for the KEK-ATF. Nuclear Instruments and Methods A. 2010;**613**:1-8. DOI: 10.1016/j.nima.2009.10.151

[41] Yang J, Sakai F, Yanagida T, Yorozu M, Okada Y, Takasago K, et al. Low-emittance electron-beam generation with laser pulse shaping in photocathode radio-frequency gun. Journal of Applied Physics. 2002;**92**:1608-1612. DOI: 10.1063/1.1487457

[42] Kim KJ. RF and space-charge effect in laser-driven RF electron guns. Nuclear Instruments and Methods A. 1989;**275**:201-208. DOI: 10.1016/0168-9002(89)90688-8

[43] Serafini L, Rosenzweig JB. Envelope analysis of intense relativistic quasilaminar beams in RF photoinjectors: A theory of emittance compensation. Physical Review E. 1997;**55**:7565-7590. DOI: 10.1103/PhysRevE.55.7565

[44] Travier C. An introduction to photo-injector design. Nuclear Instruments and Methods A. 1994;**340**:26-39. DOI: 10.1016/0168-9002(94)91278-5

[45] Yang J, Kan K, Kondoh T, Murooka Y, Naruse N, Yoshida Y, et al. An ultrashort-bunch electron RF gun. The Journal of the Vacuum Society of Japan. 2012;**42-49**(Japanese):55. DOI: 10.3131/jvsj2.55.42

[46] GPT code. General Particle Tracer. Available from: http://www.pulsar.nl/gpt

[47] Tanimura K. Femtosecond Time-Resolved Atomic Imaging. 2017. Available from: http://www.sanken.osaka-u.ac.jp/labs/aem/project.top.html201 [Accessed: 2018-08-05]